Contents lists available at *Dergipark*

Journal of Scientific Reports-A

journal homepage: *https://dergipark.org.tr/tr/pub/jsr-a*

E-ISSN: 2687-6167 ***Number 59, December 2024***

RESEARCH ARTICLE

Receive Date: 05.07.2024 *Accepted Date: 29.07.2024*

An experimental investigation of reducing the wake length at a low speed by passive flow control and biomimetic application

Sefa Şahin[a], Ahmet Selim Durna[b], Cem Kolbakır[c,*]

[a]*Department of Aerospace Engineering, University of Samsun, Samsun, Türkiye ORCID: 0000-0002-2920-5849*
[b]*Department of Aerospace Engineering, University of Samsun, Samsun, Türkiye ORCID: 0000-0002-9824-6660*
[c]*Department of Aerospace Engineering, University of Samsun, Samsun, Türkiye ORCID: 0000-0002-3355-6289*

Abstract

This study explores the use of biomimetic designs in passive flow control to reduce wake length at low speed, aiming to enhance aerodynamic efficiency. Inspired by nature's optimization of fluid dynamics in birds and marine life, this research investigates the applicability of these biological principles to improve aerospace engineering designs, particularly for low Reynolds number flows relevant to Unmanned Aerial Vehicles (UAVs). The experimental setup involved a smoke visualization wind tunnel to examine flow patterns around several wing models. These models incorporated bio-inspired elements, mimicking shark skin riblets and humpback whale tubercles, strategically positioned to delay flow separation and minimize wake length. The wing models, designed using 3D modeling software and printed via a 3D printer, were tested at various angles of attack in a smoke visualization wind tunnel by measuring their wake length via image processing. Experiments were carried out in two stages; types of protrusion were investigated on the first stage and the position of a selected protrusions examined in the second stage. The findings indicate significant differences in wake length reduction across the models, with certain biomimetic adaptations, especially optimized triangular protrusions inspired by shark skin, showing notable improvements in aerodynamic performance at higher angles of attack. Among different models in the first stage, Model B was the most effective model in aerodynamic performance with a drag reduction effect of 18% compared to the reference model NACA 0018. In the second stage experiments, Model B-15 showed the most effective aerodynamic result by reducing the wake length by 30% in the range of α=0˚-20˚, while the reduction for Model B-20 was 26%. The results offer valuable insights into the design of efficient, low-speed flight vehicles, suggesting that biomimetics could lead to innovative designs with higher performance and energy efficiency. This research emphasizes the potential of integrating biomimetic principles into passive flow control strategies.

* Corresponding author. Tel.: +90-362-313-0055 | 2134
E-mail address: cem.kolbakir@samsun.edu.tr

Keywords: biomimetics; experimental aerodynamics; passive flow control; smoke visualization; riblet; drag reduction

1. Introduction

The use of a solution inspired by living and/or inanimate objects is called bio-inspiration. It has been widely used in building design, especially in art, since the early times of humanity. It was first mentioned in 1957 by Otto Schmitt, under a scientific approach put forward to solve the problems of humans regarding systems, processes, and models in nature. It has taken its place in the literature as "biomimetic" in 1969 [1]. Although its initial application was primarily seen in architectural designs, today its usage in engineering problems has become widespread, evolving into a recognized branch of science. Its application in the field of aerodynamics started back in the 1500s with Da Vinci and has been systematically investigated over the last 40 years, and the most common examples of its application are in aircraft designed by being inspired by the body and wing structure of living things capable of flying [2].

Aviation was inspired not only by the structure of flying creatures but also by birds, insects, plants and sea creatures. The body and fin formations of sea creatures, along with their similar structure to creatures in the air, draw attention. Studies on the leaf and spiny structures of plants also show formations to reduce drag or allow the fluid to slide on a hydrophobic surface [3]. Observing birds in general, it has been proven that the wing structures, the arrangement of the feathers on the front and rear wings, and the protrusions on wing tips are used to reduce drag and achieve lower energy consumption [3,4]. Due to the movements of living things in nature, it is logical to create new designs inspired by nature, especially in small-sized aircraft like micro UAVs. The low-speed interactions that take place in living things are at where aerodynamic effects are observed, which makes development in this field reasonable. Another example is a bomber aircraft designed with inspiration from the wings, body, and tail structures of birds shown in Fig. 1 (a). Gopinathan and colleagues focused on the influence of the wavy pattern structure on whale fins experimentally. They studied under different conditions, depending on whether the wave amplitude structure is constant or variable, and its effect on the tapering wing structure. It has been observed that for wing models with different amplitude waves and a sweep angle of 30˚, the tubercles increase the lift to drag coefficient performance $(C_L/\ C_D)$ of swept-back wings by enhancing C_L/C_D ratio in the pre-stall angles of attack region [4]. As a similar example, humpback whale's wavy fin is used in the wind turbine blade and iceboat mast to support sail could be seen in Fig. 1 (b). In the Fig. 1 (c), the protruding structure (riblets) of the shark's body is used to cover the aircraft. These applications increase aerodynamic performance by connecting the flow to the wing [5].

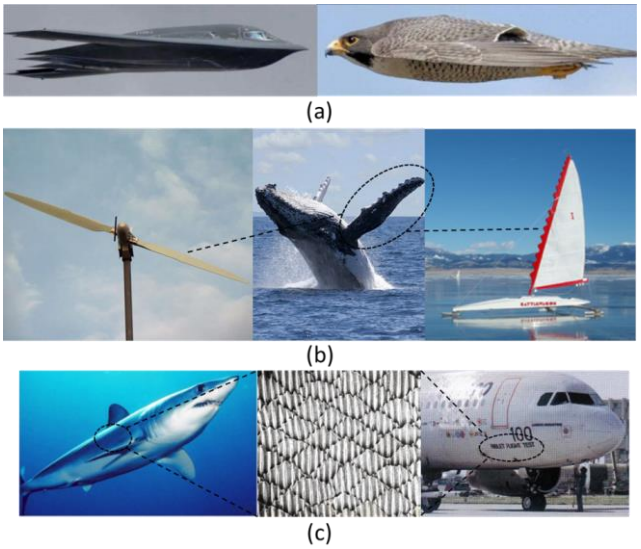

Fig.1. Biomimetic example (a) for wing and fuselage structure a B-2 Bomber inspired by stooping peregrine falcon [6] (b) wind turbine blade inspired by the fin structure of humpback whales (left) and iceboat with leading-edge tubercles on the mast supporting a sail (right) [7,8] (c) trials of shark-inspired riblets on an airplane covered with a plastic film of the same microscopic texture [3,9].

Protruding surfaces are based on the principle of preventing the flow from stalling by providing vortex formation at low speed. Due to the formation of the pressure difference, the flow attaches to the surface more, reducing drag, increasing lift, and ensuring its continuity.

The study of Stark et al. [10] examined the effect of leading-edge tubercles on the wake behaviour around a marine rudder with a NACA 0015 profile at $Re=2.26\times10^6$. The improvement in the lift coefficient reaches up to 19%. The study of Zhang et al. [11] used a novel leading-edge protuberance method at $Re=2\times10^5$ with the aim of examining the control effectiveness and associated flow physics. The lift coefficient and lift-to-drag ratio were improved by the protuberance, with increases of 54.5% and 67.7%, respectively, and decreased drag and moment coefficients, by as much as 6.70% and 11.1%. The study of Asghar et al. [12] employed a bioinspired passive flow control strategy in the leading-edge region of a propeller blade. Specific tubercle configurations exhibited improvements in efficiency of up to 6%. The study of Domel et al. [13] showed that riblets provide improvements in lift-to-drag ratio ranging from 1.2% and 4.2%. It is important to note that the flow regime considered in this study ($Re\approx4\times10^4$) is relevant for many systems. The interest in low Re (10^3-10^5) related to renewable energy (wind turbine) and aviation has increased. Unmanned and micro air vehicles are gaining importance with developing technology (military and civil). In the low Reynolds number regime, the strong effect of viscous forces leads to earlier stalling of the wing profile compared to the high Reynolds number regime [14]. Inspired by riblets, their designed surface structure provided improvements in lift-to-drag ratio comparable to those best reported. This outperforms currently available designs at low angles of attack, with improvements of up to 323%. Additionally, this study introduces a new perspective to the literature by applying 2D bump geometry to optimize biomimetics. In their study using the PIV technique, they observed that a short separation bubble developed behind both the riblet and the 2D bump geometry, helping to provide greater suction and therefore lift for these foils compared to the control. Also, as understood from the CFD results they performed by positioning

the riblet on a flat plate showed that the separation bubble and streamwise vortices created when the riblet is placed correctly on an airfoil will help increase lift force and reduce drag. Güler et al. [15] numerically investigated the aerodynamic performance of NACA 0018 by adding riblets on the side of suction at $Re=1\times10^5$. Their results revealed a 4.5% enhancement in the C_L/C_D ratio and a 37% increase in lift coefficient, due to the reduction in trailing edge separation and laminar separation bubble. The study of Han et al. [16] has demonstrated that the biomimetic shark-skin coating, fabricated using the bio-replicated forming method, achieves a significant drag reduction efficiency, reaching up to 8.25% relative to the flat surface. The study of Viswanath [17] presents experimental effects of riblets applied to wings, airfoils, and aircraft or wing-body designs. Optimized riblets achieved a skin friction drag reduction of 5–8% on 2D airfoils. In wing-body configurations, an overall drag reduction of approximately 2–3% is expected.

While research on aerodynamic effects using biomimetics is not a recent subject, its application to low-speed vehicle studies is relatively rare. However, the advances in technology are increasing the focus on low-speed applications [4,11,12,13,15]. Despite the aforementioned studies, using the smoke visualization technique in a low-speed wind tunnel, especially at low Reynolds numbers to observe the effects of biomimetic applications are quite rare. One of the known studies belongs to Seyhan et al. [18]. In the study, flow around a NACA 0015 airfoil with leading-edge tubercles was investigated using force measurements and smoke visualization at the range of $\alpha=0^\circ$-30°. Tests were performed at a low Reynolds number, specifically $Re=6.3\times10^4$. The improvement in aerodynamic performance observed as a result of the experiment is due to the presence of stall cell creation with the counter-rotating vortex couples and three-dimensional spanwise flow pattern induced by leading-edge tubercles in the post-stall regime. Present study, seeks to evaluate the aerodynamics of passive control methods, such as protrusions, biomimetics, and surface shapes, through the application of smoke visualization techniques. Various bio-inspired airfoil geometries such as 2D bumps, optimized triangular prisms, and shark skin-inspired protrusions (riblets) were analyzed by smoke visualization and by comparing their wake length.

2. Models and experimental setup

Experiments were conducted at the Aerodynamics Laboratory of the University of Samsun. The first component of the experimental setup is the smoke visualization wind tunnel, which is the TecQuipment Modular Air Flow Bench (AF17). The dimensions of the test section are 260×260×40 mm and airflow speed varies from 0.8 to 35 m/s. The produced models are securely positioned in the test section center and then angle of attack is adjusted by means of a digital protractor measuring with an accuracy of 0.01˚. LED lighting is installed along the edges of the test section, which aids in clear visualization of smoke lines, flow separations, and vortex formations during the experiments. Smoke generated by a smoke generator passes through a smoke rake into the test section. To ensure homogeneous smoke distribution, a specially designed smoke rake with needles is used. This smoke rake disperses smoke lines in a dense and thin structure, enhancing the accuracy of observations and the interpretability of results. Additional information about the smoke rake can be found in Jurnal et al. [19]. The second component of the experimental setup is the ViCount Compact Smoke Generator branded oil-based smoke generator. The experiment equipment is shown in Fig. 2. For the experiments, the wing models were designed using a computer-aided 3D modeling software and printed via a 3D printer. Polylactic Acid (PLA) printing material with a precision of 0.2 mm was utilized, using a printer with dimensions of 220×220×250 mm. The models have 100 mm chord and 40 mm span, making contact with the walls of the test section at both ends.

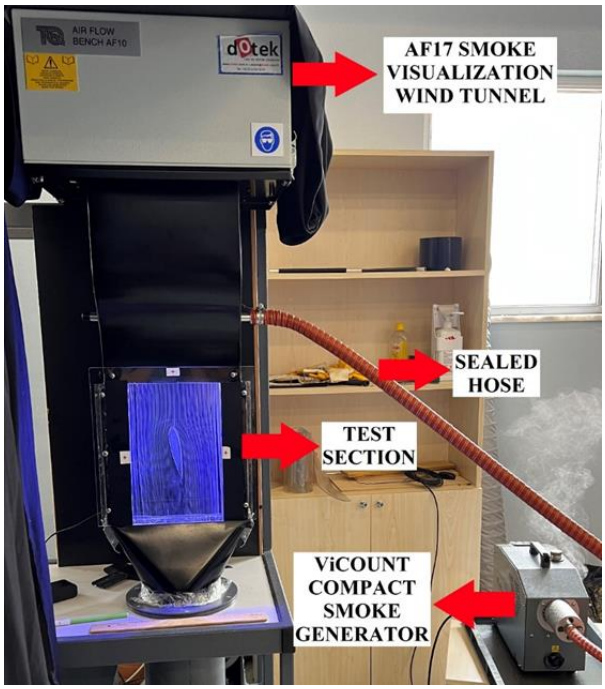

Fig. 2. Components of experimental setup.

All experiments were performed at angles of attack (α) of 0˚, 4˚, 8˚, 12˚, 14˚, 16˚ and 20˚. The experiments were carried out in two stages. Initially, five different wing structures -NACA 0018, Model A, Model B, Bump Model, and Riblet Wing Model- were tested. At the end of the first stage, the second stage experiments were conducted using Model B, which exhibited the greatest reduction in wake length across all α during the first stage. Thus, in the second stage, variations of Model B were tested and changes in wake length were evaluated through image processing. The protrusions on the models were placed at the maximum thickness of the wing and their height was adjusted to 2 mm. NACA 0018, served as a reference for measurements, while other models (Model A, Model B, Bump Model, and Riblet Wing Model) were produced and tested based on the work of Domel et al. [13], as mentioned previously. The "bump" on Bump Model was designed by scaling the upper half of the NACA 0018 airfoil geometry and placing it on the airfoil. The bump has an induced angle α=3˚. Model A, inspired from shark skin riblets, consists of optimized triangular prisms protrusions on NACA 0018 airfoil. The width of the triangular profile was set to 2 mm. These same features applied to Model B, except the triangles were 4 mm wide. The Riblet Wing Model has six riblets protrusions inspired by structure of shark skin itself. The angle between the wing model and riblets is defined as tilted angle, θ. Unlike the studies of Domel et al. [13], the upper surface of the riblet was designed as a flat surface and the riblets tilted at a much higher angle (θ = 40˚) to overcome the production difficulties. Additionally, for the second stage experiment, six models consisting of different vertical distance variations of Model B (ranging from 0.25c to the leading edge with decrements of 0.05c) were designed. Refer to Fig. 3 for images of the designed models and positive tilted angle θ for riblets. Finally, a SONY DSC-RX10MIII camera was set up in front of the smoke visualization wind tunnel to capture images during the experiment. The models at the determined angles of attack are tested multiple times with long exposure to ensure possible mishaps and the accuracy of the experiment. It has been observed that there is no difference between the images taken. The experiments are carried out and processed under the same

conditions and measurement features. Image processing was carried out via MATLAB. A non-dimensional distance reference measurement location was selected based on the 0.1c distance from the trailing edge of the wing. Since the models itself are infinite wings, there are no wing-tip effects and only 3D effects are caused by the protrusions. Number of pixels between two streamlines at the wake were measured, then calculated in terms of non-dimensionalized distance x/c. The results of repeated image processing are the same and the accuracy of the measurements taken is provided with precision. Additional information about the image processing can be found in Jurnal et al. [20].

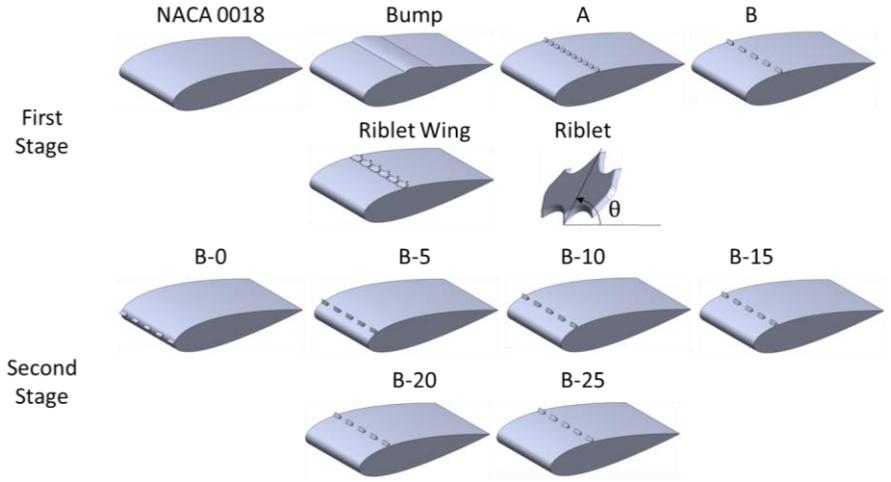

Fig. 3. Designed models and positive tilted angle θ for riblet.

3. Results and discussions

Models were tested using smoke visualization wind tunnel and performed at low Reynolds number. Some processed images of the first stage experiments -NACA 0018, Model A, Bump Model, Model B and Riblet Wing Model- are arranged side by side in Fig. 4 according to their α. The results of the experiment, show the variation of dimensionless wake length according to an α for the five models, as depicted in Fig. 5. The visualization results show that boundary layer separation is clearly visible from the streaklines as the α increases. From Fig. 4, for α=0˚, it is seen that the wake lengths of the other models, except the Riblet Wing, are very similar to each other. Streaklines attached around the models without any separation, but in the Riblet Wing, the flow passing the riblets started to disperse, and then a laminar separation bubble formed on the wing. As seen in Fig. 5, it prevented the flow from attaching to the wing, thus increasing the wake length. Streaklines on NACA 0018 between α=8˚-12˚, the separation occurs from the trailing edge to the leading edge and the wake length increases in this process. In this range, Model A and Model B induce turbulence in the flow thanks to their triangular prism protrusions. The streaklines captured by the protrusions are clearly visible for Model A at α=12˚, and for Model B at α=8˚ and 12˚. This effect seems to be more dominant in Model B than in Model A. The reason for this is that the width of the triangular prisms on Model B are twice as large as those on Model A. Due to its narrow width in Model A, it fails to suppress turbulence development, thus unable to reattach the flow behind the wing, resulting in no change in wake length. In Model B, due to its greater width, it allows turbulence to develop and effectively retains the flow around the wing, resulting in a lower wake length. When Fig. 4 in the Bump Model analyzed, the effect of inducing turbulence and retaining the flow can be clearly observed at α=8˚and 12˚. When compared in Fig. 5, the Bump Model provides a similar aerodynamic performance increase to the Model B. This effect of the Bump Model on attaching the streamlines to the wing is due to the rounded structure at the leading edge of the bump. At α=16˚, Model A, Model B, and the Bump Model cannot fully utilize the advantages

provided by their protrusions because the flow separation shifts towards the leading edge, causing the separated flow to bypass the protrusions without following the surface, indicating a loss of flow interaction. However, it is understood that a slight pressure change is created due to their protruding structures and that they still accelerate the flow and contribute to turbulence. The effect of the high θ can be seen in the Riblet Wing. The incoming flow continues to contact the riblets and still has control in the wake region. However, as seen in Fig. 5, the wake length is higher than other models due to the high θ. Compared to NACA 0018 with α=20˚, other models have a lower and similar wake length The protrusions do not disturb the flow and provide a lower wake length even if separated earlier. Thus, NACA 0018 has a higher wake length than other models. This shows that the effect of the pressure change at α=16˚ continues. The effects of α can be seen in Fig. 5. Starting from α=4˚-8˚, wake length differences between the wings began to appear. Differences before the α=4˚-8˚ are not very noticeable. Models with similar wake lengths at α=4˚ differed with the increasing angle of attack immediately afterwards. This also indicates that the protrusions located in the same position provide similar control at low α, but at higher α such as 14˚, it is observed that the B-30 model dominates in control.

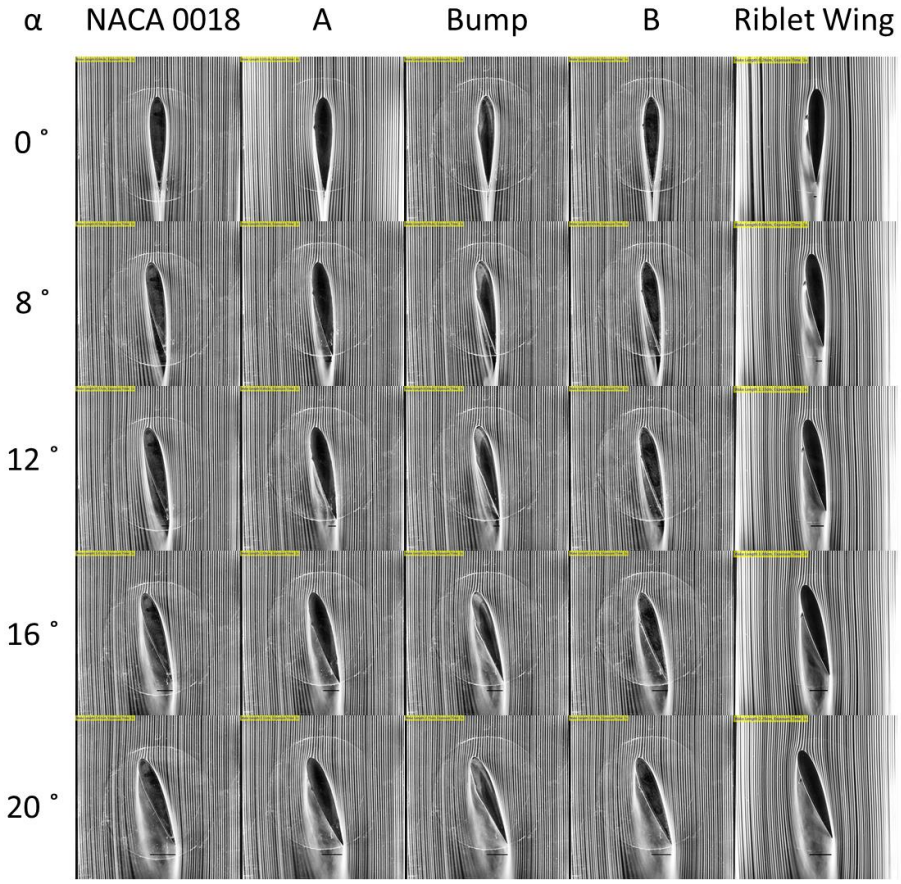

Fig. 4. Processed images of first stage models at different angles of attack.

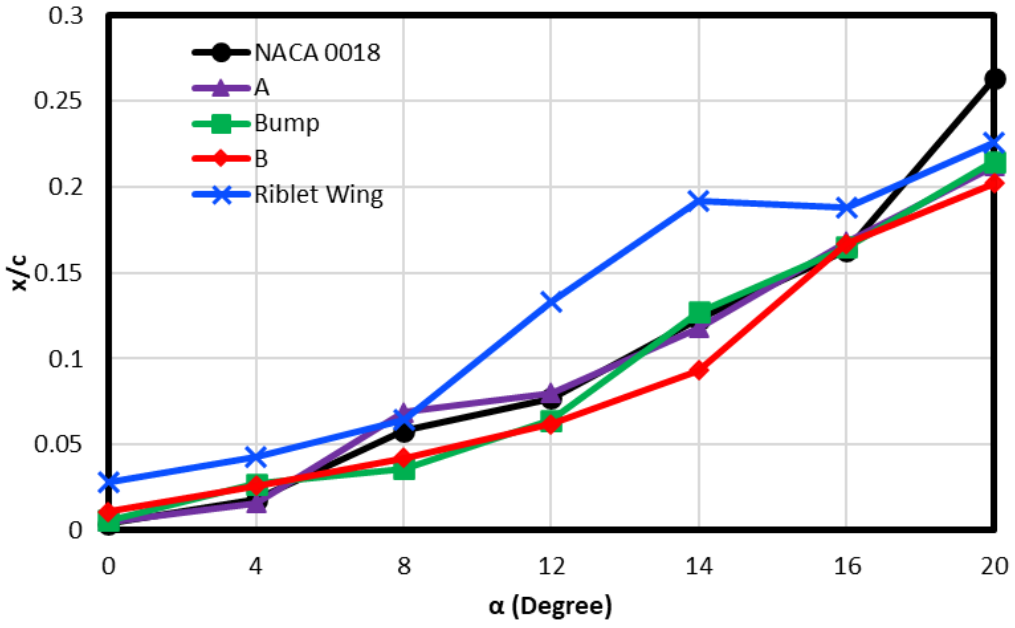

Fig. 5. Variation of dimensionless wake length according to α of 5 models in first stage experiments.

In Riblet Wing Model, a higher tilt angle was applied compared to previous studies in the literature [13]. Riblets resulted in an increase in the wake length at all angles of attack except α=20˚. It has been observed that the reason for these wake increases is the laminar separation bubble effect, particularly noticeable at α=0˚ and 4˚, as shown in Fig. 6. As mentioned by Genc and colleagues [21], in a low Reynolds number regime, as in this study, laminar separation bubble can induce an early stall by separating the flow from the wing.

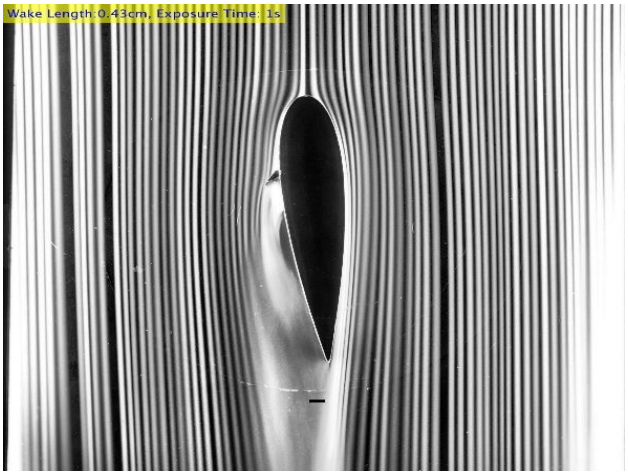

Fig. 6. Laminar separation bubble formation on Riblet Wing Model at 4˚ angle of attack.

Results of Model A generally were close to NACA 0018, as seen in Fig. 5. Results indicate a reduction in wake length by an average of 4% between α=12˚-20˚ and 7% between α=14˚-20˚. Bump Model, inspired by the work of Domel et al. [13], reduced wake length by an average of 11% between α=8˚-20˚. Despite an initial increase in wake length up to α=5˚, Bump Model was able to decrease wake length and increase aerodynamic performance within the α=4˚-14˚ range. This result aligns with the drag coefficient trend observed in the study of Domel et al. [13], indicating consistency between wake length measurement, as depicted in Fig. 5, and drag coefficient. This alignment underscores the robustness of the findings, demonstrating compatibility between qualitative and quantitative data. However, since the bump already has an α=3˚, it is more prone to stall. Consequently, Bump Model exhibited a larger wake length after α=14˚.

Among all models in the first stage experiments, Model B positively impacted performance by reducing wake length, according to Fig. 5. It exhibited the least wake length and decreased it by an average of 24% between α=8˚-14˚ and 18% between α=8˚-20˚. This shows protrusions on Model B were effective in delaying the stall. According to the experimental study by Jacobs and Sherman [22], which has a Reynolds number (Re=41,400) that is quite similar to this study, the stall angle of NACA 0018 is about 9˚. The stall angle of Model B occurs after α=14˚, indicating that it delays the stall. Therefore, as seen in Fig. 3, Model B was chosen for the second stage of the experiments instead of Model A, Bump Model and Riblet Wing. Variations of Model B were created to better examine the effects of protrusion.

Some processed images of second stage models -B-15, B-20 and B-25- from the flow visualization experiments, compared with Model B and NACA 0018, are arranged side by side according to their α in Fig. 7. Variation of dimensionless wake length according to angle of attack is given in Fig. 8. As seen in Fig. 7, at α=0˚, the flow remains attached to the surface of the wing in all models. When α=8˚, it is clearly seen that the flow in NACA 0018 begins to separate from the trailing edge, but has not entered the stall yet. A similar situation is also seen in the Model B-25. In the B-10, B-15, B-20 and B-30, it is seen that the flow is attached to the wing with the effect of the protruding structure. This ensured that the wake length was longer than NACA 0018, as seen in Fig. 8. At α=12˚, it was observed that the B-10 and B-15 exhibited a sudden increase in wake length. In the NACA 0018, it is observed that the flow begins to separate from a location further behind where the protrusions of B-10 and B-15 are located. When the B-10 and B-15 models are examined in Fig. 7 and 8; it is seen that at low α, while the flow is attached to the wing, it loses its control effect between α= 8˚-12˚ and the height of the protrusion that the flow contacts increases the flow separation area and increases the wake length. At α=16˚, it is evident that the passive flow control characteristics of the B-15 and B-25 become dominant at high angles. It is observed that the protrusions provide the flow to bring it closer to the wing. At α=20˚, the two models that are still effective appear to be B-15 and B-30. The control effects of protruding models on wake length continue, although they weaken. When analyzed in general, it has been observed that protrusions positioned close to the leading edge are effective at high α, while protrusions positioned further back are effective at low α. B-15, on the other hand, appears to play an effective role at both high and low α among the protruding models positioned in the 0-0.3c range. For other α that are not included in the images in Fig. 7, evaluation can be made in Fig. 8. The protruding models, which were similar at α=0˚ and 4˚ and provided a slightly lower wake length than NACA 0018, behaved differently as the α increased. Compared to the NACA 0018, while the B-25 initially experiences an increase in wake length, it provides a decrease at α=12˚ and 14˚. It was determined that the B-25 model triggered leading edge separation at low α (4˚-8˚), but suppressed this separation by providing flow control by showing the protrusion effect at increasing α (12˚-14˚). At the following α, wake length increased dramatically. While B-15 provides more effective control at low α such as 4˚ and 8˚, it increases wake length at 12˚ and 14˚. Subsequently, it manages to achieve lower wake length again at 16˚ and 20˚. When B-10 and B-20 are analyzed, it is seen that B-10 is effective up to 8˚ and B-20 has control superiority between α=8˚-12˚. Between 14˚-20˚, B-10 was again superior to B-20 in terms of control over wake length.

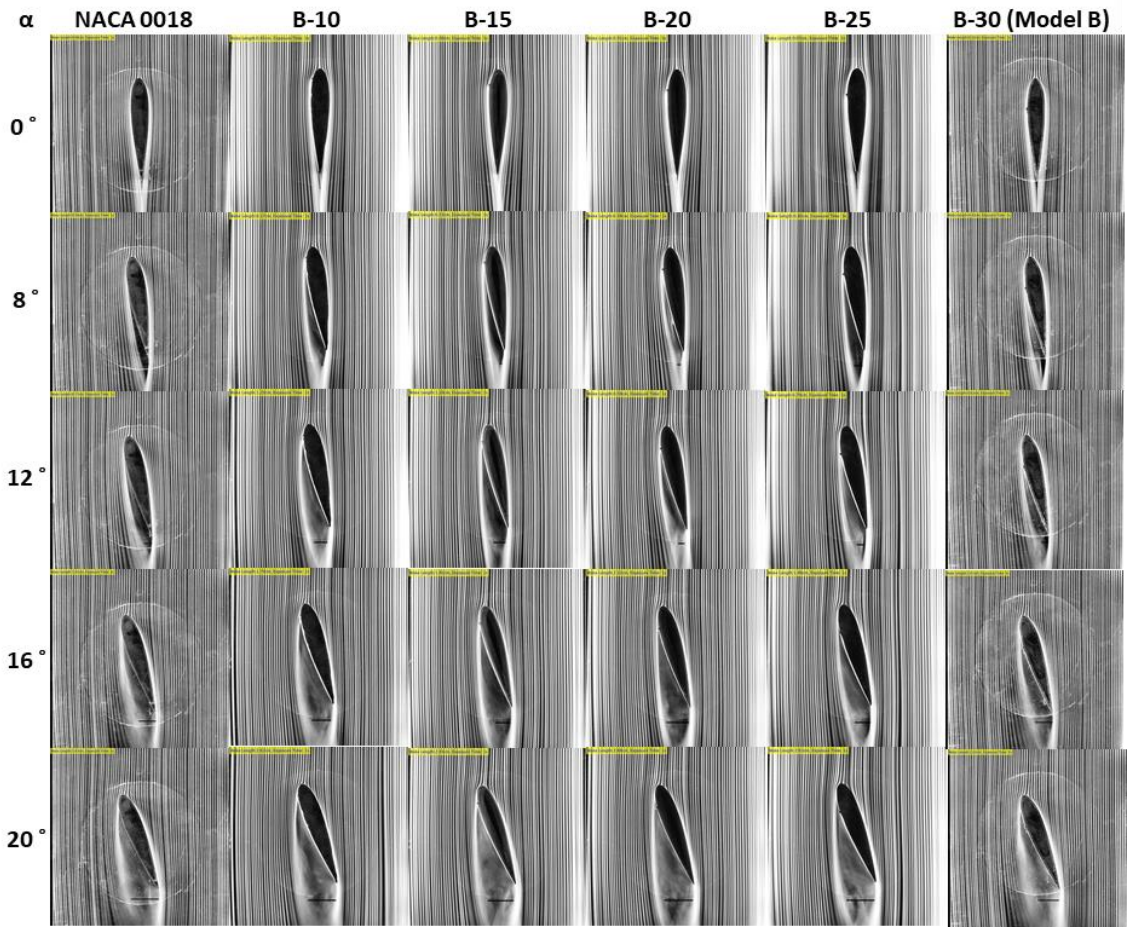

Fig. 7. Processed images of second stage models at different angles of attack.

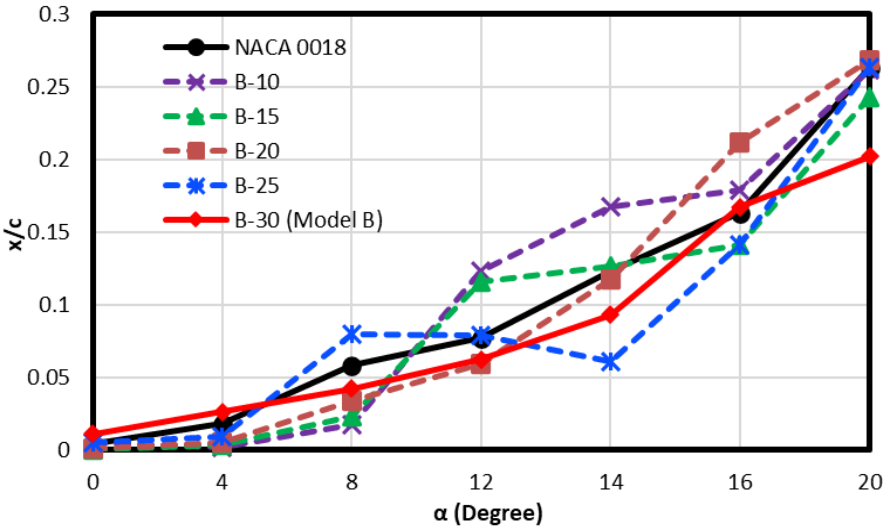

Fig. 8. Variation of dimensionless wake length according to α for second stage experiments.

Among the models presented in Fig. 3, Model B-0 and B-5 were the least effective results compared to NACA 0018. Model B-0 increased the wake length at all angles of attack except α=4˚ and a similar trend was observed in Model B-5 except α=4˚ and α=20˚. Therefore, B-0 and B-5 were excluded from Fig. 7 and 8. The aerodynamic performance of Model B-10, with the protrusions placed at 0.1c, is presented in Fig. 8. While the reduction in wake length in the range of α=0˚-8˚ is an average of 45%, this reduction decreases to only 4% in α=0˚ and 20˚ range. Model B-15 provided the most effective performance increase compared to NACA 0018 among all tested models. Wake length was reduced by an average of 30% in α=0˚-20˚. It reduced the wake length by an average of 81% in α=0˚-8˚ and by an average of 6% in α=14˚-20˚. The performance provided by the Model B-15 started to decrease again towards later models. Similar to the Model B-15, Model B-20 demonstrated high performance gains by reducing wake length. It reduced the wake length by an average of 26% in the α range of 0˚-20˚, and provided an uninterrupted reduction of an average of 43% in the α range of 0˚-14˚. The Model B-25 shows a wake length reduction of an average of 7% in the 0˚-20˚ range, similar to the Model B-10. It is effective between α=12˚-20˚ and it reduces the wake length by an average of 15%. As seen in Fig. 8 for the Model B-25, it is quite interesting that even if the angle increases α=8˚-14˚, the wake length remains almost constant between α= 8˚-12˚ and then decreases α=12˚-14˚.

4. Conclusion

Experimental studies based on biomimetics in passive flow control in smoke visualization in the wind tunnel was used to examine changes in wake length at low Reynolds numbers ($Re=3.5\times10^4$). Most of the studies in the literature are carried out with high Reynolds numbers. To the authors' knowledge there is no study has been conducted, in the fields of biomimetics, using the smoke visualization technique in a low-speed wind tunnel, especially at lower Reynolds numbers. To the authors' knowledge, studies using smoke visualization techniques in a low-speed wind tunnel, especially at low Reynolds numbers to observe the effects of biomimetic applications are quite rare. In the experiments carried out, positive effects of biomimetics and aerodynamics were observed. The study aims to understand the effect of bioinspired protruding sections and their effects on aerodynamic performance by investigating the wake length. It has been found that by causing the turbulence in the flow, the flow attaches to the wing, delaying the stall, and increasing aerodynamic performance due to the reduced wake length. Protruding structures cause

turbulence in low-speed flow, creating effects such as the flow attached to the wing, delaying stall, and improving aerodynamic performance due to the reduction in drag force. It has been observed that the protruding structure placed in the appropriate position of the wing is effective at both low and high α. We noticed that results obtained with wake length measurement methods in this study agree quite well with experimental results obtained by Domel et al. [13].

In the first stage of the experiments, 5 different models with protrusions at the thickest cross section of the airfoils were tested and evaluated by their post-stall performance. Riblet Wing Model, as a complete application of biomimetics compared to Model B, Model B is indisputably superior to the Riblet Wing Model. It can be said that the tilted angle and design of Domel et al. [13] are quite functional for riblet design. While there was no change in the wake length for Model A post-stall compared to reference NACA 0018, it was decreased by an average of 11% for Bump Model and 18% for Model B. Performance difference between Model A and B is interesting. The difference between the two models is that the widest of the triangular prisms has been increased from 2 mm to 4 mm. This creates a difference in the sequence frequency of the protruding structures. However, while this seemingly simple difference made almost no difference compared to the Reference Model NACA 0018 in one case (Model A), it provided a superior aerodynamic performance increase in the other (Model B).

Second stage experiments continued with Model B and its variations. Among the all models, Model B-15 was the design that showed the most effective aerodynamic performance. It reduced the wake length by an average of 30% in the α=0˚-20˚ range compared with NACA 0018. Model B-20, reduced its wake length by an average of 26% in the α= 0˚-20˚ range. The Riblet Wing Model increased the wake length at all angles except α=20˚. When the α increases, the flow separation approaches the leading edge. At a low α, flow separation occurs near the trailing edge, and at a high α, flow separation occurs closer to the leading edge. As can be seen from these results, the positions of the placed protrusions provide control over this phenomenon. As seen in the Model B-15 and Model B-20, this positioning is effective at both low and high α.

In future studies, when the Riblet structure, the effects of placing it on the wing at different tilted angles and the frequency of its arrangement can be investigated. The effect of the Bump Model, different wing models can be tried as bumps (such as NACA 0012 and NACA 2412). Hot wire tests can be performed in both experimental stages, taking into account these visual and wake length measurements. Thus, the results obtained from this experiment can be confirmed with more quantitative results.

Acknowledgements

The research work is supported by TÜBİTAK 2209-A (project number: 1919B012102223).

References

[1] J. F. V Vincent et al., “Biomimetics : its practice and theory Biomimetics : its practice and theory,” pp. 471–482, 2009, doi: 10.1098/rsif.2006.0127.

[2] J. B. Anders, “Biomimetic flow control,” *Fluids 2000 Conf. Exhib.*, no. June, 2000, doi: 10.2514/6.2000-2543.

[3] J. B. R. Rose, S. G. Natarajan, and V. T. Gopinathan, Biomimetic flow control techniques for aerospace applications: a comprehensive review, *Springer*, vol. 20, no. 3. Netherlands, 2021 doi: 10.1007/s11157-021-09583-z.

[4] V. T. Gopinathan, J. Bruce Ralphin Rose, and M. Surya, “Investigation on the effect of leading edge tubercles of sweptback wing at low reynolds number,” *Mech. Ind.*, vol. 21, no. 6, 2020, doi: 10.1051/meca/2020095.

[5] D. W. Bechert, G. Hoppe, and W. E. Reif, “On the drag reduction of the shark skin,” *AlAA 23rd Aerosp. Sci. Meet.* 1985, 1985, doi: 10.2514/6.1985-546.

[6] W. A. Akpan, C. M. Orazulume, E. J. Oduobuk, E. Engineering, I. State, and A. I. State, “Aerodynamics of Birds’ Flight: Analysis and Applications,” *International Journal of Applied Science and Research*, pp. 156–177, 2023.

[7] D. T. H. New and B. F. Ng, Flow Control Through Bio-inspired Leading-Edge Tubercles: Morphology, Aerodynamics, Hydrodynamics and Applications. 2020. doi: 10.1007/978-3-030-23792-9.

[8] F. E. Fish, P. W. Weber, M. M. Murray, and L. E. Howle, "Marine applications of the biomimetic humpback whale flipper," *Mar. Technol. Soc. J.*, vol. 45, no. 4, pp. 198–207, 2011, doi: 10.4031/MTSJ.45.4.1.

[9] Z. Han et al., "Biomimetic multifunctional surfaces inspired from animals," *Adv. Colloid Interface Sci.*, vol. 234, pp. 27–50, 2016, doi: 10.1016/j.cis.2016.03.004.

[10] C. Stark and W. Shi, "The influence of leading-edge tubercles on the hydrodynamic performance and propeller wake flow development of a ducted propeller," *Proc. Int. Offshore Polar Eng. Conf.*, pp. 2837–2844, 2021.

[11] M. M. Zhang, G. F. Wang, and J. Z. Xu, "Experimental study of flow separation control on a low-Re airfoil using leading-edge protuberance method," *Exp. Fluids*, vol. 55, no. 4, 2014, doi: 10.1007/s00348-014-1710-z.

[12] A. Asghar, R. E. Perez, P. W. Jansen, and W. D. E. Allan, "Application of leading-edge tubercles to enhance propeller performance," *AIAA J.*, vol. 58, no. 11, pp. 4659–4671, 2020, doi: 10.2514/1.J058740.

[13] A. G. Domel, M. Saadat, J. C. Weaver, H. Haj-Hariri, K. Bertoldi, and G. V. Lauder, "Shark skin-inspired designs that improve aerodynamic performance," *J. R. Soc. Interface*, vol. 15, no. 139, pp. 1–9, 2018, doi: 10.1098/rsif.2017.0828.

[14] J. G. Leishman, *Introduction to Aerospace Flight Vehicles*. Embry-Riddle Aeronautical University, 2022.

[15] E. Güler, T. Durhasan, İ. Karasu, and H. Akbıyık, "Passive Flow Control around NACA 0018 Airfoil Using Riblet at Low Reynolds Number," *Iğdır Üniversitesi Fen Bilim. Enstitüsü Derg.*, vol. 11, no. 3, pp. 2208–2217, Sep. 2021, doi: 10.21597/jist.897982.

[16] X. Han, D. Y. Zhang, X. Li, and Y. Y. Li, "Bio-replicated forming of the biomimetic drag-reducing surfaces in large area based on shark skin," *Chinese Sci. Bull.*, vol. 53, no. 10, pp. 1587–1592, May 2008, doi: 10.1007/s11434-008-0219-3.

[17] P. R. Viswanath, "Aircraft viscous drag reduction using riblets," 2002.

[18] M. Seyhan, M. Sarioglu and Y. E. Akansu, "Influence of Leading-Edge Tubercle with Amplitude Modulation on NACA 0015 Airfoil," *AIAA JOURNAL*, vol.59, no.10, pp.3965-3978, 2021

[19] G. Jurnal, C. Kose, C. Kolbakir, A. S. Durna, and B. Karadag, "Improvement of smoke rakes and the image processing for the flow visualization experiments," in *11th Ankara International Aerospace Conference*, September 2021, 2021, pp. 1–7.

[20] G. Jurnal, T. Çobanoğlu, C. Kolbakir, and A. S. Durna, "Flow Control Using Plasma Actuator On The Airfoils With Various Camber And Thickness Dimensions," in *ULIBTK'24 Uluslararası Katılımlı 23. Isı Bilimi ve Tekniği Kongresi*, 2023, pp. 1–10.

[21] M. S. Genç, I. Karasu, and H. Hakan Açikel, "An experimental study on aerodynamics of NACA2415 aerofoil at low Re numbers," *Exp. Therm. Fluid Sci.*, vol. 39, pp. 252–264, 2012, doi: 10.1016/j.expthermflusci.2012.01.029.

[22] E. N. Jacobs and A. Sherman, "Airfoil section characteristics as affected by variations of the Reynolds number," *Tech. rep.*, Washington. D.C Natl. Advis. Comm. Aeronaut., no. 586, pp. 227–259, 1939.